Effective Resistance of Two-Dimensional Truncated Infinite Mesh Structures

Rassul Bairamkulov, *Student Member, IEEE*, and Eby G. Friedman, *Fellow, IEEE*

***Abstract*— Determining the effective resistance of a mesh is a powerful tool for simplifying the analysis of complex electrical structures, ranging from transistors to power delivery systems. A common structure in science and engineering is a two-dimensional resistive grid. Applications of this structure include IR drop analysis and decoupling capacitor allocation in on-chip power and ground networks in VLSI systems, and the analysis of electrical and thermal conductive media, such as a semiconductor substrate. In the case where the effective resistance is evaluated far from the grid edges, an infinite resistive lattice can be used to simplify the analysis of a grid. If however the target nodes are located close to the grid edges, the assumption of infinite dimensions becomes invalid, producing inaccurate results. To bridge this gap, a resistive mesh truncated along a single or two dimensions is discussed here. Integral expressions for the effective resistance within a truncated infinite mesh structure are provided, as well as a closed-form approximation, which exhibits good agreement with the exact integral equation, exhibiting an average error of 0.27% and a maximum error of 4.77%. These expressions significantly improve the accuracy of the effective resistance estimation near the edges and corner of a resistive mesh, providing a tenfold reduction in error. In case studies, the expressions provide four to six orders of magnitude speedup in IR analysis of a $10^4 \times 10^4$ grid, while providing accuracy comparable to nodal analysis.**

***Index Terms*— Very large scale integration, resistance, power dissipation, passive circuits, graph theory, functional analysis, power distribution.**

I. Introduction

A MESH structure is an important topology for modeling a variety of physical and mathematical phenomena. The structure consists of regularly placed nodes within a multi-dimensional space and connected with resistors to adjacent nodes. Despite the theoretical nature of an infinite mesh structure, a variety of practical examples exist, where the size and regularity support the assumption of an infinite grid. For example, the resistance of a large uniform conducting sheet can be modeled as a resistive grid [1], enabling the use of an infinite resistive grid to model, for example, substrate noise [2].

Manuscript received May 22, 2019; accepted July 24, 2019. Date of publication August 30, 2019; date of current version October 30, 2019. This work was supported in part by the National Science Foundation under Grant CCF-1526466 and Grant CCF-1716091, in part by the Intelligence Advanced Research Projects Agency (IARPA) under Grant W911NF-14-C-0089, and in part by the grants from Synopsys, Cisco Systems, and Qualcomm. This article was recommended by Associate Editor Y. Sun. *(Corresponding author: Rassul Bairamkulov.)*

The authors are with the Department of Electrical and Computer Engineering, University of Rochester, Rochester, NY 14627 USA (e-mail: rbairamk@ur.rochester.edu; friedman@ece.rochester.edu).

Color versions of one or more of the figures in this article are available online at http://ieeexplore.ieee.org.

Digital Object Identifier 10.1109/TCSI.2019.2933749

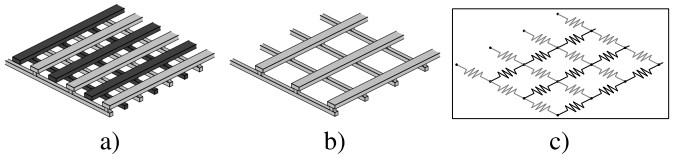

Fig. 1. Two layer power and ground network mesh modeling process. a) Original view of two-layer mesh. The light and dark gray segments are connected to, respectively, power and ground. b) A simplified model with the ground mesh removed. c) Equivalent resistive mesh of the power network.

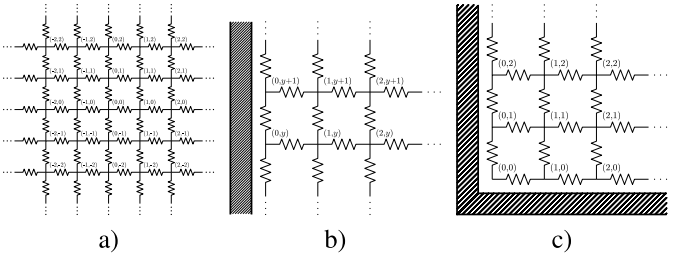

Fig. 2. Portions of two-dimensional infinite resistive structures. a) Portion of fully infinite mesh near the origin. b) Portion of half-plane mesh near the edge. c) Portion of quarter-plane mesh near the corner.

A mesh structure is prevalent in modern integrated circuits, particularly in power and ground distribution networks [3] and decoupling capacitor placement [4]. The power and ground delivery networks typically consist of layered perpendicular metal interconnects [4]. A typical on-chip network structure is shown in Fig.1a. During the analysis process, power supply and ground networks are typically analyzed separately, as shown in Fig.1b. The resulting grid can be modeled as a resistive mesh, as shown in Fig.1c.

Analysis of power delivery noise in power grids is an important problem in VLSI systems. Conventional nodal analysis tools typically exhibit superlinear computational complexity, resulting in significant simulation time. An alternative approach for the analysis of power delivery grid circuits is proposed in [5]. To simplify the analysis, the resistive mesh is reduced to an equivalent effective resistance where the grid is assumed to be infinitely large. The primary benefit of this approach is significantly lower complexity, independent of grid size. The main drawback, however, is higher error in proximity of the grid boundaries due to the assumption of an infinite grid.

This paper aims to bridge this gap. The effective resistance of a large resistive grid near the edges and corners is modeled as a truncated infinite mesh. In this paper, the infinite mesh truncated along a single dimension is called a half-plane mesh (Fig. 2a), while an infinite mesh truncated along two orthogonal dimensions is called a quarter-plane mesh (Fig. 2b).

By utilizing the image and superposition methods, exact integral and approximate closed-form expressions for half- and quarter-plane meshes are presented. A brief review of the electric potential in an infinite mesh is provided in Section II. The image method for electric circuits is described in Section III. A derivation of the exact integral equations is described in Section IV, followed by a derivation of the closed-form expressions in Section V. The accuracy of the results is discussed in Section VI. The findings are summarized in Section VII.

II. Background

Determining the effective resistance between two nodes of an infinite resistive mesh, also known as a Liebman mesh [6], is a classical problem. The objective is to determine an effective two-port resistance given a two-dimensional network with identical resistors between adjacent nodes, as shown in Figs. 2a and 2b.

The problem has been studied from a variety of perspectives. An intuitive solution for determining the effective resistance between adjacent nodes within a mesh is described in [6] and [7], where superposition of the current sources and symmetry are used to determine the voltage between adjacent nodes. The first general solution for this problem was published in 1940 [8], where the probability of reaching a specific node within a lattice during a random walk is determined, a process closely related to finding the effective resistance within a grid [9]. A solution, specific to electrical circuits, was published in 1950 [10], where a two-dimensional elliptic wave partial differential equation is applied to an infinite lattice. Several later works have been published describing alternative methods to solve this problem, including Fourier Transform [1], [11], Green's function [12] and graph theory [13].

Several extensions and variations of solutions to this problem have been published. In [11] and [12], the problem is solved for a multi-dimensional grid, and triangular and hexagonal infinite lattices. Regular and semi-regular polyhedric structures as well as multi-dimensional cubes are described in [14], and an infinite cylindrical grid is considered in [15]. More practical considerations are included in [16], where a solution for an infinite grid with unequal horizontal and vertical resistances is provided.

Despite the problem being well studied, little attention has been devoted to the effects of truncations on the effective resistance. One version for determining the effective resistance in an infinite mesh is provided in [13],

$$R_{eff}(x, y) = \frac{1}{\pi i} \int_0^{\pi} \frac{1 - e^{x \cos^{-1}(2-\cos(\alpha))} \cos(y\alpha)}{\sqrt{1 - (2 - \cos(\alpha))^2}} d\alpha. \quad (1)$$

The accuracy of (1) is compared with numerical analysis of a large resistive mesh. The relative error of the effective resistance near the edges and corners is shown, respectively, in Figs. 3 and 4. Due to the assumptions of symmetry and regularity, the effective resistance is more accurately evaluated near the center of the grid, where the effect of the boundaries is less significant. Near the edges and corners, however, the error of (1) can reach 40%, limiting the applicability of the integral expression.

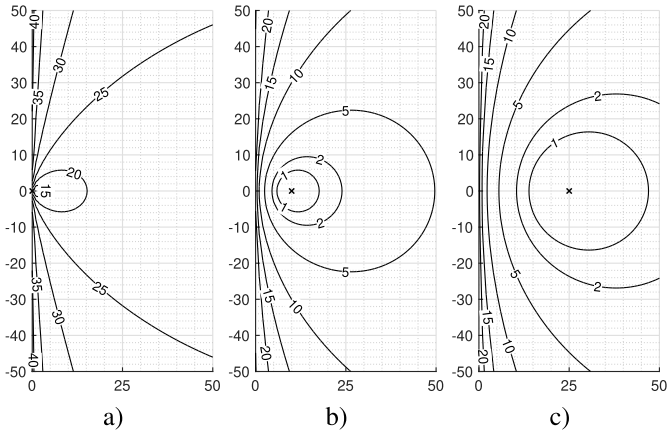

Fig. 3. Relative error (in per cent) of the effective resistance expression of an infinite grid (1) [13] within the proximity of the grid edge. The actual resistance is determined using a nodal analysis between node $(x_0, 0)$ and node (x, y) for a) $x_0 = 0$, b) $x_0 = 10$, and c) $x_0 = 25$. The grid dimensions are 101×201. The point $(x_0, 0)$ is indicated by the $\times$-mark.

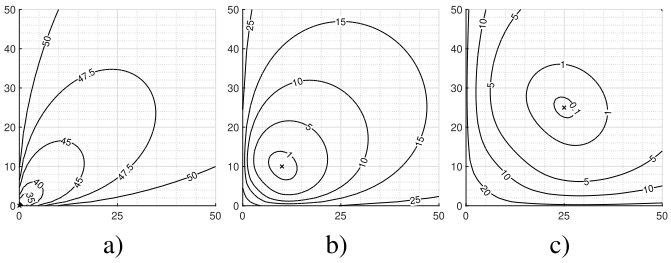

Fig. 4. Relative error (in per cent) of the effective resistance expression of an infinite grid (1) [13] within the proximity of the grid corner. The actual resistance is determined using a nodal analysis between node (x_0, y_0) and node (x, y) for a) $x_0 = y_0 = 0$, b) $x_0 = y_0 = 10$, and c) $x_0 = y_0 = 25$. The grid dimensions are 101×101. The point (x_0, y_0) is indicated by the $\times$-mark.

III. Electric Potential in an Infinite Mesh

The solution proposed in this paper is based on modifying the methods described in [13] and [16]. An alternative Green's function-based approach is presented in Appendix A. Consider a fully infinite anisotropic resistive mesh. Let the horizontal and vertical resistances be, respectively, $r_x = r$ and $r_y = kr$. Assign coordinates to each node, inject current I into node (x_0, y_0), and let the current exit at a node infinitely far from the injection node. Denote the potential at node (x, y) due to current I injected at (x_0, y_0) as $\phi_{x_0,y_0}(x, y)$. Three important properties of this potential exist. First, if the current source is moved by distance (a, b), the potential distribution across the grid is also moved by the same distance,

$$\phi_{x_0,y_0}(x, y) = \phi_{x_0+a,y_0+b}(x + a, y + b). \quad (2)$$

Another important property is symmetry, i.e., the current source and probe coordinates can be swapped,

$$\phi_{x_0,y_0}(x, y) = \phi_{x_0,y}(x, y_0) = \phi_{x,y}(x_0, y_0) = \phi_{x,y}(x_0, y_0). \quad (3)$$

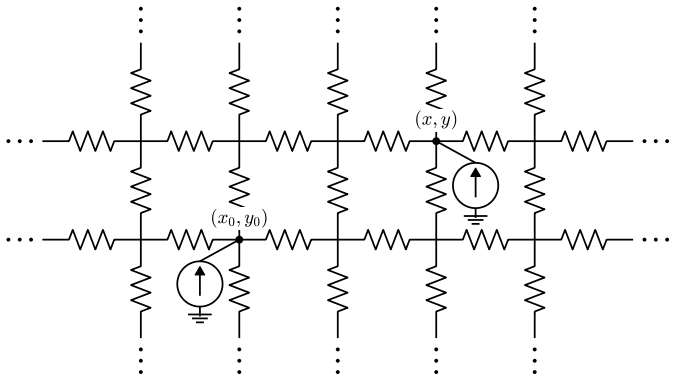

Fig. 5. Current injection into an infinite resistive mesh.

From these properties, note that

$$\begin{aligned}\phi_{x_0,y_0}(x,y) &= \phi_{-x_0,y_0}(-x,y)\\ &= \phi_{-x_0,-y_0}(-x,-y) = \phi_{x_0,-y_0}(x,-y). \quad (4)\end{aligned}$$

To evaluate the effective resistance R_{eff} between nodes (x_0, y_0) and (x, y), the two current sources can be superimposed, as shown in Fig. 5. Knowing the voltage drop between these nodes allows the effective resistance to be determined,

$$R_\infty = \frac{V_{x_0,y_0} - V_{x,y}}{I}, \quad (5)$$

where V_{x_0,y_0} and $V_{x,y}$ are the voltage, respectively, at (x_0, y_0) and (x, y). V_{x_0,y_0} and $V_{x,y}$, in turn, can be expressed as the superposition of the potentials due to multiple current sources,

$$V_{x_0,y_0} = \phi_{x_0,y_0}(x_0,y_0) - \phi_{x,y}(x_0,y_0), \quad (6)$$

$$V_{x,y} = \phi_{x_0,y_0}(x,y) - \phi_{x,y}(x,y). \quad (7)$$

Based on (2) to (7), the resistance between two arbitrary nodes is

$$R_\infty = \frac{2\big(\phi(0,0) - \phi(x-x_0, y-y_0)\big)}{I}, \quad (8)$$

where, for brevity, $\phi(x, y) = \phi_{0,0}(x, y)$.

IV. Electric Potential Within a Truncated Infinite Mesh

The solution proposed in this paper is based on modeling the mesh truncation using image current sources. The image theorem is a powerful technique widely used in electrostatics to determine the effects of surfaces on an electric field distribution. A similar technique can be utilized to determine the electric potential due to the current source near the mesh truncation. The validity of the image method for a truncated mesh is established in Appendix B using the uniqueness theorem. In subsection IV-A, the potentials of a fully infinite grid determined in section III are superimposed to model the behavior of a truncated grid. In subsection IV-B, the integral expression for the effective resistance in a half-plane and quarter-plane grid is presented.

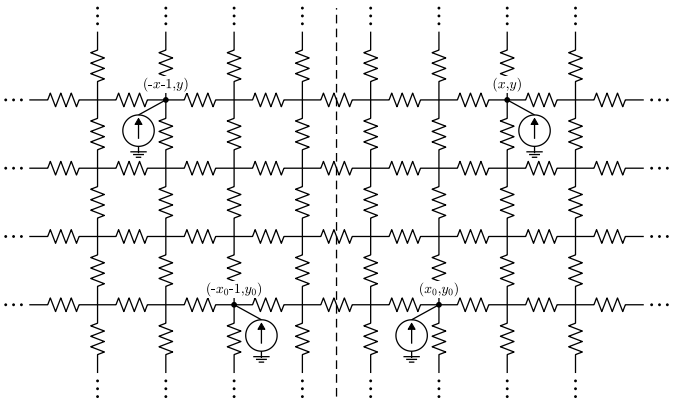

Fig. 6. Image method to model truncation in a half-plane mesh. The dashed line illustrates the boundary between the real and image half-planes. Two image sources are introduced in the negative-x plane to model the effect of truncation, ensuring zero effective current across the boundary.

A. Modeling Truncation with Image

Consider the case where an infinite grid of resistors is truncated at $x = 0$, removing all of the nodes with negative coordinates, as shown in Fig. 2. The assumption of symmetry along the x-axis becomes invalid, making the solutions reported in [8] to [12] inapplicable for a truncated mesh.

To circumvent this limitation, truncation can be replaced with another topology modification which satisfies the boundary conditions, (52) and (53). The truncated mesh structures are modeled as a fully infinite mesh with boundary conditions. The condition for the half-place mesh is

$$\phi(0,y) - \phi(-1,y) = 0, \quad (9)$$

i.e., the current flowing through the grid edge is zero. Similarly, a quarter-plane mesh is modeled as a fully infinite mesh with the following boundary conditions,

$$\phi(0,y) - \phi(-1,y) = 0, \quad (10)$$

$$\phi(x,0) - \phi(x,-1) = 0. \quad (11)$$

The image technique accomplishes this task. In the following subsections, expressions for the effective resistance in terms of potentials are derived.

1) Half-Plane Mesh: Consider the circuit topology shown in Fig. 6 with the ground placed infinitely distant. The positive-x side of the grid remains the same as the truncated grid. The symmetric negative-x side, however, maintains zero voltage between nodes $(0, y)$ and $(-1, y)$, thereby modeling the effect of the grid edge by satisfying the boundary condition (9).

A derivation of the effective resistance starts with (5). To model the truncation, two image current sources are introduced, as shown in Fig. 6. Unlike a fully infinite mesh, the voltage at nodes (x_0, y_0) and (x, y) within a half-plane mesh is the sum of the potential due to four current sources,

$$\begin{aligned}V_{x_0,y_0} &= \phi_{x_0,y_0}(x_0,y_0) - \phi_{x,y}(x_0,y_0)\\ &\quad + \phi_{-x_0-1,y_0}(x_0,y_0) - \phi_{-x-1,y}(x_0,y_0), \quad (12)\\ V_{x,y} &= \phi_{x_0,y_0}(x,y) - \phi_{x,y}(x,y)\\ &\quad + \phi_{-x_0-1,y_0}(x,y) - \phi_{-x-1,y}(x,y). \quad (13)\end{aligned}$$

Simplifying (2) to (4),

$$V_{x_0,y_0} = \phi(0,0) - \phi(x-x_0, y-y_0) + \phi(2x_0+1,0) - \phi(x+x_0+1, y-y_0), \quad (14)$$

$$V_{x,y} = \phi(x-x_0, y-y_0) - \phi(0,0) + \phi(x+x_0+1, y-y_0) - \phi(2x+1,0). \quad (15)$$

Combining (14) and (15) with (5) yields

$$R_{half} I = 2\phi(0,0) - 2\phi(x-x_0, y-y_0) + \phi(2x_0+1,0) - 2\phi(x+x_0+1, y-y_0) + \phi(2x+1,0). \quad (16)$$

2) Quarter-Plane Mesh: Consider the case shown in Fig. 2, where an infinite mesh is truncated along the x- and y-axes. Similar to the half-plane case, this topology can be modeled by introducing six image current sources, as shown in Fig. 7, thereby satisfying the boundary conditions in (10) and (11). The resulting voltages at (x_0, y_0) and (x, y) are the sum of the potentials due to eight current sources, which, after simplification, yields

$$\begin{aligned} V_{x_0,y_0} &= \phi(0,0) + \phi(2x_0+1,0) \\ &\quad + \phi(0,2y_0+1) + \phi(2x_0+1, 2y_0+1) \\ &\quad - \phi(x-x_0, y-y_0) - \phi(x+x_0+1, y-y_0) \\ &\quad - \phi(x-x_0, y+y_0+1) - \phi(x+x_0+1, y+y_0+1), \end{aligned} \quad (17)$$

$$\begin{aligned} V_{x,y} &= \phi(x-x_0, y-y_0) + \phi(x+x_0+1, y-y_0) \\ &\quad + \phi(x-x_0, y+y_0+1) + \phi(x+x_0+1, y+y_0+1) \\ &\quad - \phi(0,0) - \phi(2x+1,0) - \phi(0,2y+1) - \phi(2x+1, 2y+1). \end{aligned} \quad (18)$$

The effective resistance is, therefore,

$$\begin{aligned} R_{qt.} I &= 2\phi(0,0) + \phi(2x_0+1,0) \\ &\quad + phi(0,2y_0+1) + \phi(2x_0+1, 2y_0+1) + \phi(2x+1,0) \\ &\quad + \phi(0,2y+1) + \phi(2x+1, 2y+1) \\ &\quad - 2\phi(x-x_0, y-y_0) - 2\phi(x+x_0+1, y-y_0) \\ &\quad - 2\phi(x-x_0, y+y_0+1) - 2\phi(x+x_0+1, y+y_0+1). \end{aligned} \quad (19)$$

Expressions (16) and (19) describe, respectively, the effective resistance in a half-plane mesh and a quarter plane mesh. By adding the electric potentials at certain nodes due to the current injected at $(0,0)$, the effective resistance can be determined. Derivation of the electric potential is presented in the upcoming subsection.

B. Integral Expressions for Effective Resistance

The integral expression for the effective resistance in an anisotropic infinite grid is determined in [11] and [16] and is

$$R_\infty = \frac{kr}{\pi} \int_0^\pi \frac{1 - e^{-|x-x_0|\alpha} \cos(|y-y_0|\beta)}{\sinh(\alpha)} d\beta, \quad (20)$$

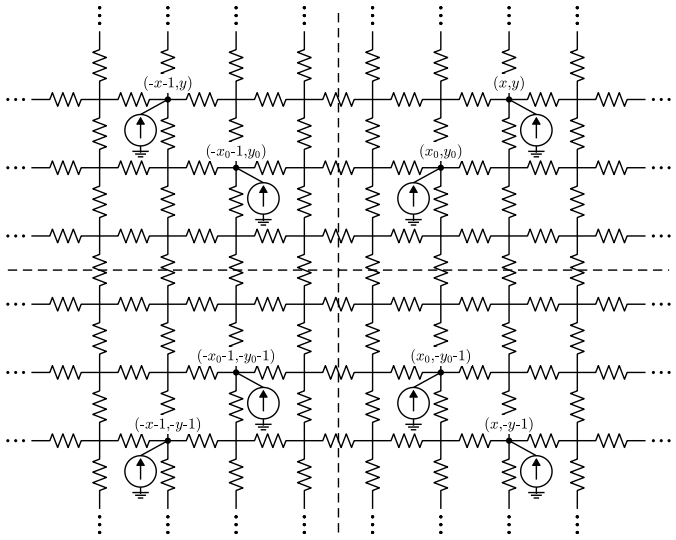

Fig. 7. Image method to model truncation in a quarter-plane mesh. The dashed lines illustrate the boundary between the real and image portions of the circuit. Six image sources are introduced in three quadrants of an infinite plane to model the effect of the truncations, ensuring zero effective current across the boundaries.

where

$$\alpha = \cosh^{-1}(1 + k - k\cos(\beta)). \quad (21)$$

$\Omega_k(x, y)$ is defined as

$$\Omega_k \equiv \frac{k}{2\pi} \int_0^\pi \frac{1 - e^{-|x|\alpha} \cos(y\beta)}{\sinh(\alpha)} d\beta. \quad (22)$$

The potential within an infinite grid (8) is described as

$$\phi(x-x_0, y-y_0) = \phi(0,0) - rI\Omega_k(x-x_0, y-y_0). \quad (23)$$

Expression (16), therefore, reduces to

$$\frac{R_{half}}{r} = 2\Omega_k(x-x_0, y-y_0) + 2\Omega_k(x+x_0+1, y-y_0) - \Omega_k(2x_0+1,0) - \Omega_k(2x+1,0). \quad (24)$$

Note that due to symmetry along the y-axis, the effective resistance of a half-plane mesh depends upon $(y - y_0)$ and not on y and y_0 separately. In contrast, both x and x_0 are necessary due to the symmetry broken by the truncation.

The exact value of (24) for the special case of $x_0 = 0$, $k = 1$ is listed in Table I. Note that due to truncation, the effective resistance in the x and y directions is not equal, with the resistance along the y-axis increasing at a higher rate. A similar trend is observed for $x_0 > 0$. The effective resistance is evaluated using (24) for $x_0 = \{0, 5, 10\}$, $x \in [0, 25]$, $y \in [-25, 25]$, and $k = 1$. The results are shown in Fig. 8. Note that the effective resistance to those nodes near the edge of the mesh is higher. Intuitively, this behavior can be explained by the more difficult access to the points along the edges. While the nodes located along the x-axis $(x, 0)$ receive current from all four sides, the nodes located along the y-axis $(0, y)$ are more difficult to reach due to there being only three sides.

TABLE I

EXACT NORMALIZED RESISTANCE BETWEEN $(0, y_0)$ AND (x, y) IN A HALF-PLANE RESISTIVE GRID WITH $y \in [-3, 3]$, $x \in [0, 3]$, AND $r_h = r_y = r$. THE NUMERICAL VALUES ARE WITHIN THE SQUARE BRACKETS

$\lvert y - y_0 \rvert$ \ x	0	1	2	3
0	0 [0.000]	$\frac{8}{\pi} - 2$ [0.546]	$\frac{856}{3\pi} - 90$ [0.824]	$\frac{128224}{15\pi} - 2720$ [0.998]
1	$\frac{2}{\pi}$ [0.637]	$\frac{18}{\pi} - 5$ [0.730]	$\frac{998}{3\pi} - 105$ [0.891]	$\frac{131854}{15\pi} - 2797$ [1.029]
2	1 [1.000]	$\frac{56}{3\pi} - 5$ [0.942]	$\frac{952}{3\pi} - 100$ [1.010]	$\frac{130208}{15\pi} - 2762$ [1.100]
3	$4 - \frac{26}{3\pi}$ [1.241]	$\frac{86}{3\pi} - 8$ [1.125]	$\frac{4766}{15\pi} - 100$ [1.138]	$\frac{43514}{5\pi} - 2769$ [1.187]

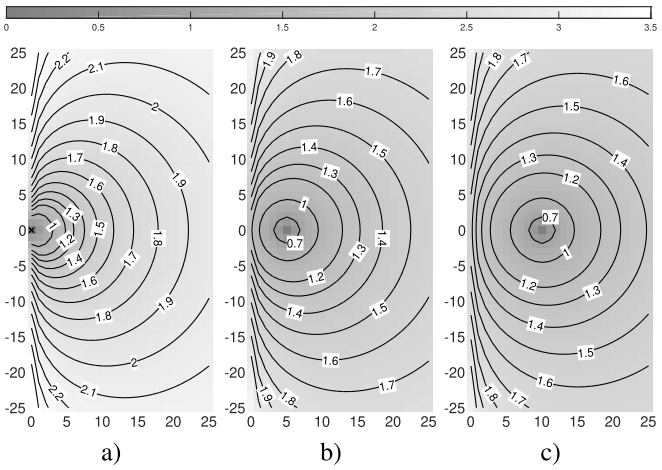

Fig. 8. Effective resistance of a half-plane mesh with $k = 1$ between $(x_0, 0)$ and (x, y) for $x \in [0, 25]$ and $y \in [-25, 25]$. a) $x_0 = 0$, b) $x_0 = 5$, and c) $x_0 = 10$.

For the quarter-plane mesh, combining (22) with (19) yields

$$\begin{aligned}\frac{R_{qt.}}{r} &= 2\Omega_k(x{-}x_0, y{-}y_0) + 2\Omega_k(x{+}x_0{+}1, y{-}y_0) \\ &\quad + 2\Omega_k(x{-}x_0, y{+}y_0{+}1) + 2\Omega_k(x{+}x_0{+}1, y{+}y_0{+}1) \\ &\quad - \Omega_k(2x_0{+}1, 0) - \Omega_k(0, 2y_0{+}1) - \Omega_k(2x_0{+}1, 2y_0{+}1) \\ &\quad - \Omega_k(2x{+}1, 0) - \Omega_k(0, 2y{+}1) - \Omega_k(2x{+}1, 2y{+}1).\end{aligned} \tag{25}$$

Note that due to the broken symmetry in both the x and y directions, the coordinates of both (x_0, y_0) and (x, y) are necessary to determine the effective resistance.

A numerical evaluation of (25) for $k = 1$ is shown in Fig. 9. As compared to the edges, the effective resistance increases more rapidly near the corner. This trend can be explained using the same intuition: the corner node can be accessed from only two sides unlike the other nodes, which can be accessed from three or four sides. Less current can therefore flow through the node at the same voltage, resulting in a higher effective resistance.

V. CLOSED-FORM APPROXIMATION

The exact resistance for a half- and quarter-plane mesh is determined from, respectively, (24) and (25). For practical purposes, however, an approximate, computationally efficient expression is desirable. A closed-form expression for the integral solution is therefore presented in this section. The

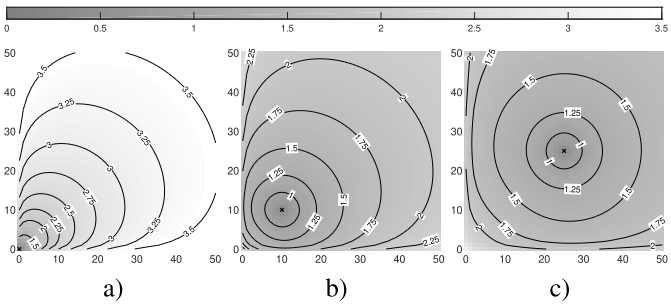

Fig. 9. Effective resistance of a quarter-plane mesh with $k = 1$ between (x_0, y_0) and (x, y) for $x \in [0, 50]$ and $y \in [-50, 50]$. a) $x_0 = y_0 = 0$, b) $x_0 = y_0 = 10$, and c) $x_0 = y_0 = 25$.

derivation is performed in two steps. First, the integral expression for the potential at an arbitrary node within a grid is approximated. The total resistance of a truncated grid is next evaluated using an approximate potential expression.

The derivation of a closed-form expression for the effective resistance is performed in two steps adapted from [1]. First, the integral expression $\Omega_k(x, y)$ is decomposed as

$$\Omega_k(x, y) = J_1 + J_2 + J_3, \tag{26}$$

where

$$\begin{aligned}J_1 &= \frac{\sqrt{k}}{2\pi}\Re\left[E_1\left(\pi\left(x\sqrt{k} + iy\right)\right)\right. \\ &\quad \left. + \ln\left(\pi\left(x\sqrt{k} + iy\right)\right) + \gamma\right],\end{aligned} \tag{27}$$

$$J_2 = \frac{k}{2\pi}\int_0^{\pi}\left(\frac{e^{-x\beta\sqrt{k}}}{\beta\sqrt{k}} - \frac{e^{-x\alpha}}{\sinh(\alpha)}\right)\cos(y\beta)d\beta, \tag{28}$$

$$J_3 = \frac{k}{2\pi}\int_0^{\pi}\left(\frac{1}{\sinh(\alpha)} - \frac{1}{\beta\sqrt{k}}\right)d\beta, \tag{29}$$

$$E_1(z) = \int_z^{\infty}\frac{e^{-t}}{t}dt, \tag{30}$$

and $\gamma \approx 0.5772$ is the Euler-Mascheroni constant. The first integral J_1 can be numerically determined using the exponential integral function $E_1(z)$, available in most popular engineering packages, including SciPy [17] and MATLAB [18]. For large values of x and y, the integral J_1 reduces to

$$J_1 \approx \frac{\sqrt{k}}{4\pi}\left[\ln\left(x^2 + ky^2\right) + 2\ln(\pi) + 2\gamma\right]. \tag{31}$$

To analyze the second integral, note that for small β, $\sinh(\alpha) \approx \beta$ and, for large values of β, the numerator of the integral vanishes for large β with values x and y

TABLE II
COEFFICIENTS FOR THE POLYNOMIAL APPROXIMATION OF J_3 (32)

Case / i	$1 \le k \le 5$	$5 \le k \le 50$
0	4.7480×10^{-2}	2.5590×10^{-2}
1	-5.9890×10^{-2}	-3.3560×10^{-2}
2	8.1530×10^{-4}	-1.0780×10^{-2}
3	-1.2740×10^{-5}	2.2600×10^{-3}
4	9.0920×10^{-8}	-1.6690×10^{-4}

above 10. This term is, therefore, neglected in the closed-form expression.

The third integral is a function of a single variable k and is approximated as a fourth degree polynomial,

$$J_3 \approx \sum_{i=0}^{4} a_i k^i, \tag{32}$$

where the coefficients of the expression are listed in Table II. The final closed-form expression for $\Omega_k(x, y)$ is, therefore,

$$\Omega_k^*(x, y) = \frac{\sqrt{k}}{4\pi}\left[\ln\left(x^2 + ky^2\right) + 2\ln(\pi) + 2\gamma\right] + \sum_{i=0}^{4} a_i k^i. \tag{33}$$

With a closed-form expression for $\Omega(x, y)$, the effective resistance of a half-plane resistive mesh is

$$\frac{R_{half}}{r} \approx 2\Omega_k^*(x - x_0, y - y_0) + 2\Omega_k^*(x + x_0 + 1, y - y_0) - \Omega_k^*(2x_0 + 1, 0) - \Omega_k^*(2x + 1, 0). \tag{34}$$

Similarly, for the quarter-plane mesh,

$$\begin{aligned}\frac{R_{qt.}}{r} \approx\ & 2\Omega_k^*(x-x_0, y-y_0) + 2\Omega_k^*(x+x_0+1, y-y_0) \\ & + 2\Omega_k^*(x - x_0, y+y_0+1) + 2\Omega_k^*(x+x_0 + 1, y+y_0+1) \\ & - \Omega_k^*(2x_0+1, 0) - \Omega_k^*(0, 2y_0+1) - \Omega_k^*(2x_0+1, 2y_0+1) \\ & - \Omega_k^*(2x + 1, 0) - \Omega_k^*(0, 2y + 1) - \Omega_k^*(2x + 1, 2y + 1).\end{aligned} \tag{35}$$

VI. MODEL EVALUATION

The primary contribution of this paper is the accurate and fast estimation of the IR drop between nodes located close to a grid edge. To evaluate the applicability of the model, in subsection VI-A, the accuracy of the exact expressions (24) and (25), closed-form expressions (34) and (35), and nodal analysis is compared. In subsection VI-B, the computational speed of the model is examined.

A. Accuracy Evaluation

The relationship between the relative error and the position of the probed nodes is shown in Figs. 10 and 11. Note that a larger error is produced when the resistance is evaluated between nearby nodes and with nodes along the y-axis. A peak error of 4.77% is produced when the resistance is evaluated between the adjacent nodes. For a large distance between $(x_0, 0)$ and (x, y), the relative error approaches zero.

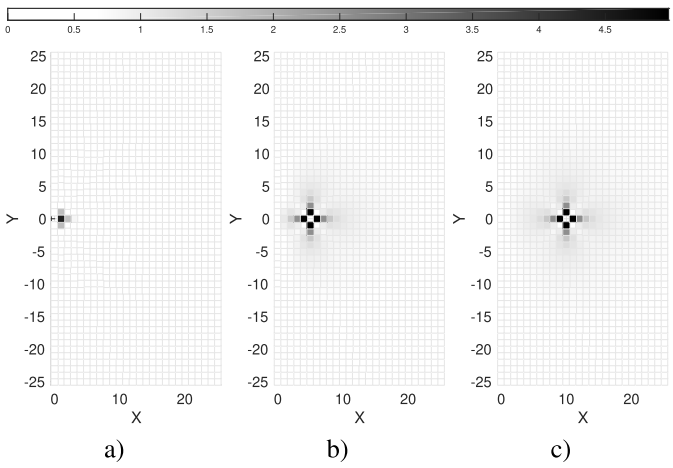

Fig. 10. Relative error (in per cent) of (34) as compared to (24) with respect to x and y for $k = 1$ and a) $x_0 = 0$,b) $x_0 = 5$, and c) $x_0 = 10$.

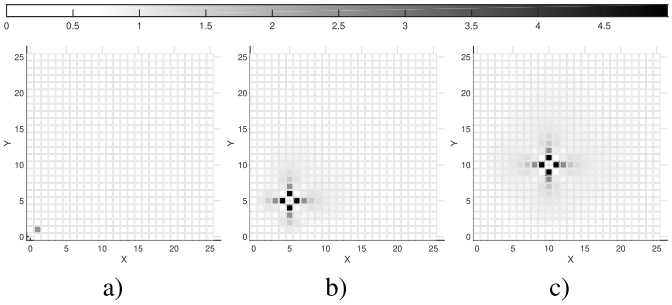

Fig. 11. Relative error (in per cent) of (35) as compared to (25) with respect to x and y for $k = 1$ and a) $x_0 = y_0 = 0$,b) $x_0 = y_0 = 5$, and c) $x_0 = y_0 = 10$.

Note from Fig. 3 that a large error is induced if the expression for a fully infinite grid is used to estimate the voltage drop near the edge of a finite mesh. A drastic increase in accuracy is observed when using (24) or (34). The error of (24) and (34) as compared to the resistance evaluated through a nodal analysis on a 101×201 mesh is shown in Fig. 12. As compared to (1), the error in (24) and (34) is below 3% along the edge. A considerably larger error is produced by (34) as compared to (24) when one of the nodes is at the grid edge and another node is in close proximity. In addition, the error is significantly increased when the effective resistance is evaluated using closed-form expression (34) between nodes within close proximity. Note that the closed-form expression is derived with the assumption of a large separation between the target nodes, which leads to larger error. In other cases, the accuracy of (24) and (34) is approximately equal. Likewise, a significant increase in accuracy is achieved with (25) or (35), as is evident from Fig. 13. Near the corner and edges, the error is below 2%.

B. Computational Speed

The speedup of the analysis and simulation process is an important contribution of this paper. The conventional method

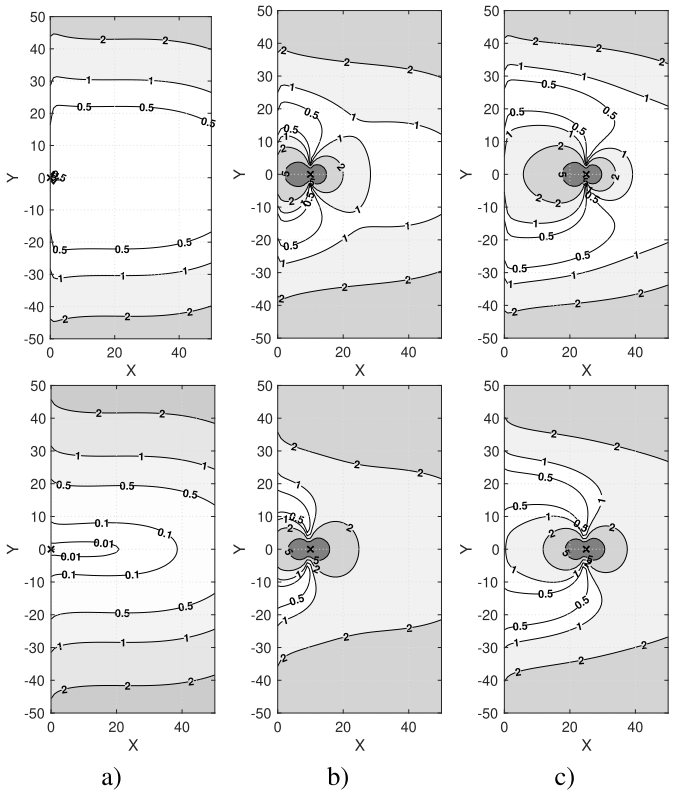

Fig. 12. Relative error (in per cent) of (24) (top row) and (34) (bottom row) as compared to the resistance determined using a nodal analysis between node $(x_0, 0)$ and node (x, y) for a) $x_0 = 0$, b) $x_0 = 10$, and c) $x_0 = 25$. The grid dimensions are 101×201. The point $(x_0, 0)$ is indicated by the $\times$-mark.

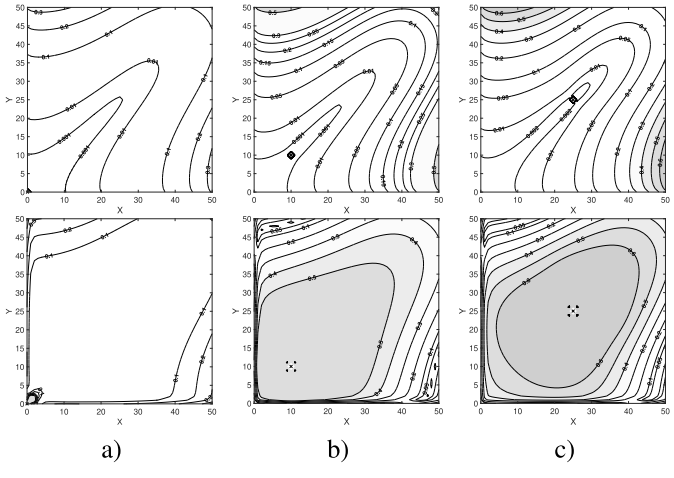

Fig. 13. Relative error (in per cent) of (25) (top row) and (35) (bottom row) as compared to the resistance determined using a nodal analysis between node (x_0, y_0) and node (x, y) for a) $x_0 = y_0 = 0$, b) $x_0 = y_0 = 10$, and c) $x_0 = y_0 = 25$. The grid dimensions are 101×101. The point (x_0, y_0) is indicated by the $\times$-mark.

for determining the effective resistance is numerical nodal analysis, where a linear system of equations is analyzed [19],

$$R_{eff} = \mathbf{1} diag(H)^T + diag(H)\mathbf{1}^T - 2H, \tag{36}$$

where $H \in \mathbb{R}^{(MN-1)\times(MN-1)}$ is the inverse of the reduced conductance matrix, $\mathbf{1} \in \mathbb{R}^{(MN-1)}$ is the vector with all entries equal to 1, and $diag(A)$ is the diagonal of matrix A. The advantage of this method is the effective resistance between any pair of nodes in a circuit can be evaluated. If the resistance between only a small subset of nodes is needed, however, this approach is highly inefficient. Assuming the pitch of the top metal layer is 2 μm for a 45 nm technology node [20], the grid size of the power delivery network in a 4 cm^2 die size is on the order of $10^4 \times 10^4$. The nodal analysis of this matrix requires the solution of a $10^8 \times 10^8$ linear system, resulting in significant analysis time. The computational time t_{nodal} required to determine the effective resistance in a nonuniform grid using nodal analysis is therefore a superlinear function of the dimensions of the grid,

$$t_{nodal} = t_1 (MN)^c, \tag{37}$$

where M and N are dimensions of the grid, t_1 is a proportionality constant, and c is the degree of the solver complexity, typically larger than one. Importantly, the method allows the effective resistance between all pairs of nodes to be determined.

In contrast, the method proposed in this paper does not require solving a system of linear expressions. The time required to determine the effective resistance using the proposed method does not depend on the grid dimensions. The method proposed here has constant complexity where the total computational time t_{image} is

$$t_{image} = t_2 n, \tag{38}$$

where n is the number of target node pairs for which the effective resistance is required, and t_2 is the time required to compute the effective resistance for a single pair of nodes using (24), (25), (34), or (35). The proposed approach is justified, therefore, when the subset of nodes of interest is sufficiently smaller than the total grid size.

TABLE III

COMPUTATIONAL SPEEDUP FOR DETERMINING THE EFFECTIVE RESISTANCE BETWEEN A PAIR OF NODES IN AN $M \times N$ GRID

Grid Size	t_{nodal}	Speedup (exact)		Speedup (closed-form)	
		R_{half}	R_{qrt}	R_{half}	R_{qrt}
$10^2 \times 10^2$	1.252 ms	1.375	0.296	11.47	8.888
$10^3 \times 10^2$	9.646 ms	11.51	1.936	227.3	80.12
$10^3 \times 10^3$	60.32 ms	53.83	5.739	1278	712.6
$10^4 \times 10^3$	462.4 ms	536.2	43.61	9062	5621
$10^4 \times 10^4$	10.85 s	7216	517.0	232148	135018

A comparison of the computational speed is provided in Table III. The algorithms are implemented in Python using the Numpy and Scipy packages [17] on an eight core 3.40 GHz Intel Core i7-6700 machine with 24 GB RAM. The nodal analysis has been performed using the Scipy sparse matrix solver [17]. Note the rapid increase in speedup with grid size. For the exact integral equations, the speedup reaches three to four orders of magnitude in a $10^4 \times 10^4$ grid. Greater speedup is achieved with the closed-form expressions, exhibiting six orders of magnitude improvement in computational time in a $10^4 \times 10^4$ grid. Simulation of grids larger than $10^4 \times 10^4$ is not possible using the Scipy sparse matrix solver due to limited memory.

VII. Conclusions

Image and superposition methods are utilized to investigate truncated infinite anisotropic mesh structures. Exact integral and closed-form expressions for the effective resistance are presented. A closed-form expression offers a computationally efficient method for evaluating the effective resistance, which can be beneficial in several VLSI circuit applications such as resistive noise analysis, placement of decoupling capacitors, and substrate noise models. Significant speedup is achieved using the proposed expressions, reaching six orders of magnitude with the closed-form expressions. The proposed framework can be utilized in a variety of VLSI oriented applications, including circuit optimization, analysis, and synthesis.

Appendix A
Green's Function for the Truncated Grid

It is of interest to determine the lattice Green's function (LGF) for a truncated infinite mesh. The LGF is the response of a lattice to a unit perturbation at the origin,

$$\Delta_r G(x, y) = \delta(x, y); \quad x, y \in \mathbb{Z}, \tag{39}$$

where $G(x, y)$ is the LGF, Δ_r is the discrete differential operator, and $\delta(x, y)$ is the Kronecker delta function, which is unity at the origin and zero elsewhere. The electrical form of (39) is obtained by applying KCL,

$$\Delta_r \phi(x, y) = r I_0 \delta(x, y); \quad x, y \in \mathbb{Z}, \tag{40}$$

where

$$\phi(x, y) = r I_0 G(x, y) \tag{41}$$

is the potential distribution within the grid in response to a current I_0 injected at the origin. Combining (8) and (41) results in

$$R_{eff} = 2r\left(G(0, 0) - G(x - x_0, y - y_0)\right), \tag{42}$$

which is consistent with [12]. From [16], the LGF for an anisotropic infinite grid is

$$G(x, y) = \frac{k}{2\pi} \int_0^{\pi} \frac{e^{-|x|\alpha} \cos y\beta}{\sinh \alpha} d\beta. \tag{43}$$

To determine the LGF for a half-plane mesh, the following equation,

$$\Delta_r \phi_{half}(x, y) = r I_0 \delta(x, y); \quad x \in \mathbb{N}_0, \ y \in \mathbb{Z}, \tag{44}$$

is solved by the image method. Expression (44) is transformed into

$$\Delta_r \phi_{half}(x, y) = r I_0 (\delta(x, y) + \delta(-x - 1, y)); \quad x \in \mathbb{N}_0, \ y \in \mathbb{Z}. \tag{45}$$

Due to the linearity of Δ_r,

$$\Delta_r \phi_{half}(x, y) = \Delta_r \phi(x, y) + \Delta_r \phi(-x - 1, y); \quad x \in \mathbb{N}_0, \ y \in \mathbb{Z}. \tag{46}$$

By the uniqueness theorem,

$$\phi_{half}(x, y) = \phi(x, y) + \phi(-x - 1, y); \quad x \in \mathbb{N}_0, \ y \in \mathbb{Z}. \tag{47}$$

Using (22),

$$\phi(x, y) = \phi_0 - r I_0 \Omega_k(x, y); \, x, y \in \mathbb{Z}, \tag{48}$$

$$\phi_0 = \frac{k I_0 r}{2\pi} \int_0^{\pi} \frac{d\beta}{\sinh \alpha}. \tag{49}$$

Expression (47) reduces to

$$\phi_{half}(x, y) = 2\phi_0 - r I_0 (\Omega_k(x, y) + \Omega_k(-x - 1, y)); \quad x \in \mathbb{N}_0, \ y \in \mathbb{Z}. \tag{50}$$

Following similar steps for the quarter-plane mesh yields

$$\phi_{qt.}(x, y) = 4\phi_0 - r I_0 (\Omega_k(x, y) + \Omega_k(-x - 1, y) + \Omega_k(x, -y - 1) + \Omega_k(-x - 1, -y - 1)); \quad x, y \in \mathbb{N}_0. \tag{51}$$

The effective resistance is determined in each case using (8).

Appendix B
Uniqueness Based on Boundary Conditions

To demonstrate the validity of the method for a truncated mesh, it is proved here that the potentials within the circuit are uniquely determined by the boundary conditions. Thus, it is sufficient to maintain the same boundary conditions while modifying the topology to ensure the same electric potentials within a grid.

Consider the circuit shown in Fig. 2a. Boundary conditions $\phi_b(x, y)$ are imposed on a set of nodes $(x, y) \in S_v$. The arbitrary node (x_g, y_g) is connected to ground. The resulting boundary conditions of the system can be expressed as

$$\phi(x, y) = \phi_b(x, y), \quad \text{at } (x, y) \in S_v, \tag{52}$$

$$\phi(x_g, y_g) = 0. \tag{53}$$

Suppose current $I_{in}(x, y)$ is injected at specific nodes $(x, y) \in S_i$ such that

$$I(x, y) = \begin{cases} I_{in}(x, y), & \text{at } (x, y) \in S_i, \quad \text{(54a)} \\ 0 & \text{otherwise.} \quad \text{(54b)} \end{cases}$$

The uniqueness theorem states that the conditions described in (52) to (53) are sufficient to uniquely determine the potential $\phi(x, y)$ due to injected current $I(x, y)$. To prove this statement, assume this statement is incorrect and two distinct distributions of potentials exist that satisfy the boundary conditions:

$$\phi_1(x, y) \neq \phi_2(x, y). \tag{55}$$

Applying Kirchhoff's current law yields

$$I(x, y) = 4\phi_1(x, y) - \phi_1(x - 1, y) - \phi_1(x + 1, y) - \phi_1(x, y - 1) - \phi_1(x, y + 1), \tag{56}$$

$$I(x, y) = 4\phi_2(x, y) - \phi_2(x - 1, y) - \phi_2(x + 1, y) - \phi_2(x, y - 1) - \phi_2(x, y + 1). \tag{57}$$

Suppose that $\phi_3(x, y)$ is also a potential distribution such that

$$\phi_3(x, y) = \phi_1(x, y) - \phi_2(x, y). \tag{58}$$

From (56) and (57),

$$0 = 4\phi_3(x, y) - \phi_3(x-1, y) - \phi_3(x+1, y) - \phi_3(x, y-1) - \phi_3(x, y+1). \quad (59)$$

Expression (59) indicates that $\phi_3(x, y)$ is the potential distribution within a circuit without current injection. No currents, therefore, flow through the resistors and $\phi_3(x, y)$ is constant. Note that

$$\phi_3(x_1, y_1) = \phi_1(x_1, y_1) - \phi_2(x_1, y_1) = 0. \quad (60)$$

Therefore, since $\phi_3(x, y)$ is constant,

$$\phi_3(x, y) = \phi_3(x_1, y_1) = 0, \quad (61)$$

$$\phi_1(x, y) = \phi_2(x, y), \quad (62)$$

which contradicts (55), indicating that the conditions described in (52) to (53) uniquely determine the potential distribution in an infinite grid due to current injection $I(x, y)$.

REFERENCES

[1] G. Venezian, "On the resistance between two points on a grid," *Amer. J. Phys.*, vol. 62, no. 11, pp. 1000–1004, Nov. 1994.

[2] Y. Ogasahara, M. Hashimoto, T. Kanamoto, and T. Onoye, "Measurement of supply noise suppression by substrate and deep N-well in 90 nm process," in *Proc. Solid-State Circuits Conf. (A-SSCC)*, Nov. 2008, pp. 397–400.

[3] I. P. Vaisband, R. Jakushokas, M. Popovich, A. V. Mezhiba, S. Köse, and E. G. Friedman, *On-Chip Power Delivery and Management*. Cham, Switzerland: Springer, 2016.

[4] M. Popovich, M. Sotman, A. Kolodny, and E. G. Friedman, "Effective radii of on-chip decoupling capacitors," *IEEE Trans. Very Large Scale Integr. (VLSI) Syst.*, vol. 16, no. 7, pp. 894–907, Jul. 2008.

[5] S. Köse and E. G. Friedman, "Efficient algorithms for fast IR drop analysis exploiting locality," *Integration*, vol. 45, no. 2, pp. 149–161, Mar. 2012.

[6] R. E. Aitchison, "Resistance between adjacent points of Liebman mesh," *Amer. J. Phys.*, vol. 32, no. 7, p. 566, Jul. 1964.

[7] E. M. Purcell, *Electricity and Magnetism*. New York, NY, USA: McGraw-Hill, 1963.

[8] W. H. McCrea and F. J. W. Whipple, "XXII.—Random paths in two and three dimensions," *Proc. Roy. Soc. Edinburgh*, vol. 60, no. 3, pp. 281–298, Jan. 1940.

[9] P. G. Doyle and J. L. Snell, *Random Walks and Electrical Networks*, vol. 22. Washington, DC, USA: Mathematical Association of America, 1984.

[10] B. van der Pol and H. Bremmer, *Operational Calculus Based on the Two-Sided LaPlace Integral*. Cambridge, U.K.: Cambridge Univ. Press, 1950.

[11] D. Atkinson and F. J. Van Steenwijk, "Infinite resistive lattices," *Amer. J. Phys.*, vol. 67, no. 6, pp. 486–492, Jun. 1999.

[12] J. Cserti, "Application of the lattice Green's function for calculating the resistance of an infinite network of resistors," *Amer. J. Phys.*, vol. 68, no. 10, pp. 896–906, Oct. 2000.

[13] K. Brown, *Infinite Grid of Resistors*. [Online]. Available: https://www.mathpages.com/home/kmath668/kmath668.htm

[14] J. T. Moody, "Efficient methods for calculating equivalent resistance between nodes of a highly symmetric resistor network," Major Qualifying Project, Worcester Polytech. Inst., Worcester, MA, USA, Tech. Rep. E-project-032913-185209, Mar. 2013.

[15] M. Jeng, "Random walks and effective resistances on toroidal and cylindrical grids," *Amer. J. Phys.*, vol. 68, no. 1, pp. 37–40, Jan. 2000.

[16] S. Köse and E. G. Friedman, "Effective resistance of a two layer mesh," *IEEE Trans. Circuits Syst., II, Exp. Briefs*, vol. 58, no. 11, pp. 739–743, Nov. 2011.

[17] (2014). *SciPy—SciPy V1.3.0 Reference Guide*. Accessed: Aug. 20, 2019. [Online]. Available: https://docs.scipy.org/doc/scipy/scipy-ref-1.3.0.pdf

[18] *MATLAB 2019a Documentation*, MathWorks, Natick, MA, USA, 2019.

[19] F. Dörfler and F. Bullo, "Kron reduction of graphs with applications to electrical networks," *IEEE Trans. Circuits Syst. I, Reg. Papers*, vol. 60, no. 1, pp. 150–163, Jan. 2013.

[20] K. Chang, K. Acharya, S. Sinha, B. Cline, G. Yeric, and S. K. Lim, "Power benefit study of monolithic 3D IC at the 7 nm technology node," in *Proc. IEEE/ACM Int. Symp. Low Power Electron. Design*, Jul. 2015, pp. 201–206.

Rassul Bairamkulov (S'17) received the B.Eng. degree in electrical and electronic engineering from Nazarbayev University, Astana, Kazakhstan, in 2016, and the M.S. degree in electrical engineering from the University of Rochester, Rochester, NY, USA, in 2018, where he is currently pursuing the Ph.D. degree under the supervision of Prof. E. G. Friedman.

He was an Intern with Qualcomm, Inc., San Diego, CA, USA, in 2018. His current research interests include power delivery network design, electronic design automation, and optimization algorithms in very large scale integration.

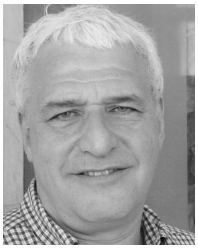

Eby G. Friedman (F'00) received the B.S. degree from the Lafayette College, Easton, PA, USA, in 1979, and the M.S. and Ph.D. degrees in electrical engineering from the University of California at Irvine, Irvine, CA, USA, respectively, in 1981 and 1989.

He was with Hughes Aircraft Company, Los Angeles, CA, USA, from 1979 to 1991, rising to Manager of the Signal Processing Design and Test Department, where he was responsible for the design and test of high performance digital and analog ICs. He has been with the Department of Electrical and Computer Engineering, University of Rochester, Rochester, NY, USA, since 1991, where he is currently a Distinguished Professor and also the Director of the High Performance VLSI/IC Design and Analysis Laboratory. He is also a Visiting Professor with the Technion—Israel Institute of Technology, Haifa, Israel. He has authored more than 500 papers and book chapters, 19 patents, and authored or edited 18 books in the fields of high-speed and low-power CMOS design techniques, 3-D design methodologies, high speed interconnect, and the theory and application of synchronous clock and power distribution networks. His current research and teaching interests include high performance synchronous digital and mixed-signal microelectronic design and analysis with application to high speed portable processors, low power wireless communications, and server farms.

Dr. Friedman was a member of the Circuits and Systems Society Board of Governors, and a program and technical chair of several IEEE conferences. He is a Senior Fulbright Fellow, a member of the Technion Board of Governors, and the UC Irvine Engineering Hall of Fame. He was a recipient of the IEEE Circuits and Systems Mac Van Valkenburg Award, the IEEE Circuits and Systems Charles A. Desoer Technical Achievement Award, the University of Rochester Graduate Teaching Award, and the College of Engineering Teaching Excellence Award. He was the Editor-in-Chief and the Chair of the Steering Committee of the IEEE TRANSACTIONS ON VERY LARGE SCALE INTEGRATION (VLSI) SYSTEMS, the Regional Editor of the *Journal of Circuits, Systems and Computers*, an Editorial Board Member of the PROCEEDINGS OF THE IEEE, the IEEE TRANSACTIONS ON CIRCUITS AND SYSTEMS II: ANALOG AND DIGITAL SIGNAL PROCESSING, *Analog Integrated Circuits and Signal Processing*, the IEEE JOURNAL ON EMERGING AND SELECTED TOPICS IN CIRCUITS AND SYSTEMS, and the *Journal of Signal Processing Systems*. He is the Editor-in-Chief of the *Microelectronics Journal*, an Editorial Board Member of the *Journal of Low Power Electronics* and the *Journal of Low Power Electronics and Applications*, and a technical program committee member of numerous conferences.